

DOI: 10.1002/((please add manuscript number))

Article type: Full paper

Anisotropic growth of non-layered CdS on MoS₂ monolayer for functional vertical heterostructures

*Wei Zheng, Wei Feng, Xin Zhang, XiaoShuang Chen, Guangbo Liu, Yunfeng Qiu, Tawfique Hasan, Pingheng Tan, PingAn Hu**

W. Zheng, W. Feng, X. Chen, G. Liu, Y. Qiu, Prof. P. A. Hu

Key Laboratory of Micro-systems and Micro-structures Manufacturing of Ministry of Education, Harbin Institute of Technology, Harbin 150080, P. R. China.

Email: hupa@hit.edu.cn

W. Zheng, W. Feng, Prof. P. A. Hu

School of Materials Science and Engineering, Harbin Institute of Technology, Harbin, 150080, P. R. China

X. Zhang, Prof P.H. Tan

State Key Laboratory of Superlattices and Microstructures, Institute of Semiconductors, Chinese Academy of Sciences, Beijing 100083, P. R. China

Dr T. Hasan

Cambridge Graphene Centre, University of Cambridge, Cambridge, CB3 0FA, UK

Keywords: epitaxial growth, CdS/MoS₂ heterostructure, photodetector, responsivity

Two dimensional (2D) semiconductors have emerged as a crucial material for use in next generation optoelectronics. Similar to micro-electronic devices, 2D vertical heterostructures would most likely be the elemental components for future nanoscale electronics and optoelectronics. To date, the components of mostly reported 2D van der Waals heterostructures are restricted to layer crystals. In this communication, we demonstrate that non-layered semiconductors of CdS can be epitaxially grown on to 2D layered MoS₂ substrate to form a new quasi vertical heterostructure with clean interface by chemical vapor deposition.

Photodetectors based on this CdS/MoS₂ heterostructure show broader wavelength response and ~50 fold improvement in photoresponsivity, compared to the devices fabricated from MoS₂ monolayer only. This research opens up a way to fabricate a variety of functional quasi heterostructures from non-layer semiconductors.

1. Introduction

Semiconductor heterostructures play a crucial role in modern microelectronics and optoelectronics^[1]. Heterostructures, combining different materials, show bandgap offset and tunable electrical and optoelectrical properties. Conventional heterostructures are primarily based on group IV, III-V, or II-VI semiconductors, with covalent bonding between atoms at the hetero-interface.^[1, 2] The usage of material components for conventional heterostructures is strongly dictated by lattice mismatch which determines the interface quality and thus, the heterostructure performance. Beyond the traditional group IV, III-V, or II-VI semiconductors, two-dimensional layered crystals (*e.g.* graphene^[3], transition metal dichalcogenides (TMDs)^[4], hexagonal boron nitride (*h*-BN)^[5], phosphorene^[6]*etc*) have emerged as promising candidates for next generation electronics and optoelectronics due to their unique properties. These 2D layered materials can be artificially combined to fabricate various van der Waals (vdW) heterostructures without the lattice match limitation. Novel physical properties of these vdW heterostructures have been investigated theoretically and experimentally, and devices based on those new heterostructures such as tunnel transistors and sensors have already been demonstrated^[7-11].

Thus far, these vdW heterostructures have mainly been fabricated by a top-down process of manual transfer or a bottom up method of chemical vapor deposition (CVD) growth. The first

demonstration of vdW heterostructures were realised by vertically stacking different 2D materials (graphene/*h*-BN^[8, 12], MoS₂/Graphene^[10], Graphene/WS₂^[9]etc) using conventional PMMA-mediated transfer method^[7]. The physical properties of these heterostructures are significantly influenced by the relative orientation of the layers and interfacial quality between them. However, the stacking style and crystal orientation cannot be easily controlled by mechanical transfer method. In addition, such strategies cannot ensure good interfacial quality. Compared to manual transfer, CVD epitaxial growth is a powerful approach for fabricating 2D vdW heterostructures with controlled stacking style, crystal orientation and clean interface. Indeed, using this strategy, some vertical heterostructures have already been successfully grown, including graphene/*h*-BN^[13], MoS₂/*h*-BN^[14], MoSe₂/graphene^[15], MoS₂/graphene^[16], WS₂/MoS₂^[17] and MoS₂/SnS₂^[18].

Thus far, the components of the reported 2D-vertical vdW heterostructures have been restricted to layered materials with planar crystal structures. However, many non-layered materials such as cadmium sulfide (CdS) also exhibit attractive optoelectronic properties^[19]. Combination of such non-layered functional semiconductors with layered materials (e.g. MoS₂) could create a new type of vdW heterostructure to provide novel platform for applications in nanoscale electronics and optoelectronics. These non-layered materials typically incline to stack into three dimensional (3D) nanostructures due to their chain-like structure and the lack of driving force for 2D anisotropic growth. We note that some non-layered materials such as noble metals, metal oxides and metal chalcogenides can be confined to 2D anisotropic growth to form sheet-like nanomaterials through the assistance of organic surfactants via wet chemical synthesis^[20]. However, these soluble sheet-like ultrathin

nanomaterials cannot be used for device applications as they become easily folded, crumpled or aggregated when they are transferred onto substrates during device fabrication. In addition, these surface-ligand protected nanosheets are not suitable for the fabrication of clean interfaces. To realize these novel vdW heterostructures with high quality interface, direct anisotropic growth of non-layered semiconductors on layered 2D materials through a CVD process is the most realistic approach. However, such a process is yet to be demonstrated.

In this work, we demonstrate epitaxial growth of non-layered CdS nanosheet on ultrathin MoS₂, creating a new vdW vertical heterostructure. We find that anisotropic growth of CdS on MoS₂ is driven by kinetics within a certain reaction temperature range influenced by the substrates, without forming energetically favored 3D structures. Photodetectors based on this CdS/MoS₂ heterostructure show broader wavelength response and significantly improved photoresponsivity compared to the devices fabricated from monolayer MoS₂ only.

2. Results and Discussion

Figure 1 shows the schematic representation of epitaxial growth of two-dimensional CdS/MoS₂ vertical heterostructures (further information in Figure S1). In the first stage, the left zone and MoO₃ zone in the furnace are heated to 250 °C and 670 °C, respectively. Subsequently, sulfur is pushed into the left zone quickly and kept for 25~30 mins. This stage is used to grow MoS₂. In the second stage, the zone of substrate containing as-grown MoS₂ cools down to 500~600 °C, meanwhile CdS zone is heated to 950 °C. Finally the CdS stream is submitted using Ar gas to the surface of MoS₂ to form the vertical heterostructure.

The as-grown triangular MoS₂ nanoflakes with sizes of up to 30 μm lateral dimension are uniformly distributed over the substrate. Such a typical MoS₂ flake is shown in Figure 2a. Figure 2b shows a scanning electron microscope (SEM) image of the vertical heterostructures, in which the dark part of the image represents a MoS₂ nanocrystal and the bright triangles or hexagons are epitaxial CdS nanosheets. The CdS/MoS₂ heterostructures are further characterized using atomic force microscopy (AFM), (Figure 2c, 2d, S2). The thickness of the epitaxial CdS on MoS₂ is in the range of 10~60 nm. Figure 2c shows an AFM image of a hexagonal CdS crystal, with ~50 nm uniform thickness. In Figure 2d, MoS₂ and CdS nanosheets with corresponding thicknesses of 1 nm and 30 nm can be observed on SiO₂/Si. Since CdS has two different crystal structures,^[21] it is necessary to determine their crystallographic phase using X-ray diffraction (XRD). In Figure 2e, the blue plot represents the XRD result of MoS₂, the red plot shows CdS powder XRD patterns from the database (PDF#41-1049), while the black plot is that of the CdS/MoS₂ heterostructure. The diffraction pattern of the heterostructure can be perfectly indexed on the database of a hexagonally phased CdS and MoS₂.

To explore the effects of MoS₂ on the growth of CdS, the CdS/MoS₂ heterostructure is studied by transmission electron microscopy (TEM) (shown in Figure 3a and Figure S3). Under TEM observation, the CdS sheets exhibit a deeper color while the MoS₂ films are almost transparent. A typical selected area electron diffraction (SAED) pattern (Figure 3b) is taken from the area of CdS/MoS₂ heterostructure (circle in Figure 3a). In this SAED pattern, two sets of six-fold symmetric diffraction spots are observed, in which the brighter and inner spots correspond to CdS (a=4.14Å) while the weaker set belongs to MoS₂ (a=3.14 Å). By

correlating the SAED pattern with the morphology (Figure 3a), the planes of the hexagonal CdS can be identified (Figure 3a), indicating that every plane of CdS is parallel to the corresponding MoS₂ plane, *e.g.* CdS (100) || MoS₂ (100) and CdS (110) || MoS₂ (110). Figure 3c and 3d show the Fourier transform high-resolution TEM of CdS and MoS₂ which were measured from the red and blue squares in Figure 3a, respectively. Both CdS and MoS₂ exhibit high quality crystallinity. The results indicate that the spacings of (100) and (110) planes of CdS are 0.36 nm and 0.21 nm, while the planes of MoS₂ are 0.27 nm and 0.16 nm respectively. These TEM characterization further demonstrate the good epitaxy of CdS on MoS₂ without any mis-orientation. Lattice mismatch between hexagonal CdS and MoS₂ is calculated to be 32% using the relationship $f = [d_{\text{CdS}}(100) - d_{\text{MoS}_2}(100)] / d_{\text{MoS}_2}(100)$,^[22] where $d_{\text{CdS}}(100) = 0.359$ nm, $d_{\text{MoS}_2}(100) = 0.272$ nm. This lattice mismatch is larger compared to traditional group IV, III-V, or II-VI semiconductor heterostructures^[23]. vdW epitaxy allows formation of high quality heterostructure consisting of two crystals with such large lattice mismatch because of the weak vdW interaction at the interface. We note that this is also applicable to manually stacked crystals. The cross-sectional electron microscope images with the clean interfaces without significant interlayer atomic mixing is shown in Figure 3e, guaranteeing the heteroepitaxial stacking. In addition, as shown in the SEM image in Figure S4, the CdS nanosheets show parallel edges, as indicated by the blue and red lines. This crystal orientation alignment (CdS (100) || MoS₂ (100) and CdS (110) || MoS₂ (110)) is attributed to vdW epitaxy. Based on the above discussion, we present a scheme of epitaxially grown CdS on MoS₂ in Figure 3f. This shows that hexagonal CdS is grown parallel to the (001) plane

surface of MoS₂ in the six equivalent directions (such as 110), rather than the preferential direction of (001). We propose that this growth kinetics is induced by the MoS₂ substrate.

To further investigate our proposal on the anisotropic growth of CdS by substrate induced kinetics, a controlled experiment is performed on the growth of CdS nanocrystals on SiO₂/Si under identical reaction parameters. This produces rod-like CdS nanocrystals, clearly showing an energetically favorable growth direction of (001) of hexagonal crystals (Figure S5). This substrate dependent growth can be well-understood by its surface energy E_s or its attachment energy E_a . A smaller value of E_s ensures higher stability while a larger $|E_a|$ indicates a faster growth process. The value of E_s and $|E_a|$ of (001)_{CdS}, calculated by Ref^[21] are much higher than any other CdS plane. This indicates that the surface of (001)_{CdS} is more active, with much faster growth rate than any other face under normal condition. This is why compared to the growth of CdS on MoS₂ (Figure 2b). CdS tripod nanocrystal is predominantly grown on SiO₂/Si (Figure S5a). Indeed the growth rate of the legs along the (001) crystallographic orientation on SiO₂/Si is much higher than that along the other surfaces. (The model of tripod nanocrystal is shown in Figure S6). On the other hand, the shapes grown on MoS₂ are different due to the substrate lattice structure and the energy barrier for nucleation (ΔG^*) at the growth temperature. Reference^[24] has recently discussed growth kinetics on layered crystals that explains our observation. According to classical nucleation kinetics, the free energy change for nucleation at heterostructures can be written as follows:

$$\Delta G_{r,\gamma} = \pi r^2 t \Delta G_v + \pi r^2 (\gamma_c + \gamma_{sc} - \gamma_s) + 2\pi r t \gamma_{c,edge}.$$

^[24] Here r and t are radius and thickness of nucleus of CdS. γ_s , γ_c , γ_{sc} and $\gamma_{c,edge}$ represent the E_s of the substrate (MoS₂ or SiO₂ in our case), E_s of the nucleus of the CdS crystals, interfacial energy between the nucleus and the substrate and the

E_s of nucleus edge of CdS crystals, respectively. The difference in free energy per unit volume during nucleation is expressed as ΔG_v . The maximum point $\Delta G_{r,\gamma}$ in the total Gibbs free energy corresponds to the critical free energy barrier for nucleation $\Delta G^* = \pi r (\gamma_{c,edge})^2 / [\Delta G_v - (\gamma_c + \gamma_{sc} - \gamma_s) / t]$.^[24] The term $(\gamma_c + \gamma_{sc} - \gamma_s)$ represents the effective change in E_s during the nucleation and is largely dependent on the growth substrate. The surface energy of MoS₂ is $\sim 70-75$ mJ/m².^[25] On the other hand, CdS grown on SiO₂ forms tripod structures due to the significantly larger E_s of the substrate ($\gamma_{SiO_2} \sim 300-400$ mJ/m²).^[26] This indicates that a larger free energy barrier must be overcome for CdS growth on SiO₂/Si compared to the epitaxial growth of CdS on MoS₂ surface. We also note that, the CdS growth is further impacted by the reaction temperature. Above 1000 °C, CdS nanocrystals always grow in energetically favorable (001) direction on both the SiO₂ and MoS₂ substrates, forming rod-like nanocrystals (Figure S5b). This is mainly attributed to the high concentration of precursor and the enhanced activity of CdS is at such high temperature (>1000 °C). Due to the grow rate increases faster along the (001) plane compared to that of the (100) plane under high temperature, the CdS nanocrystals tend to develop a rod-like morphology. Therefore, tripod-like structures (Figure S5b) rather than nanosheets (Figure 2b) of CdS nanocrystals are observed on MoS₂ surface for high temperature growth.

Raman and photoluminescence (PL) are effective ways to characterize the crystal quality and band gap these materials. The CdS/MoS₂ heterostructures (A hexagonal CdS on MoS₂ in Figure 4a and triangular CdS on MoS₂ in Figure S7) are characterized by Raman and PL with a 488 nm laser. The Raman mapping of CdS 1LO mode at 300 cm⁻¹ is shown in Figure 4b. The blue hexagon in the centre is the CdS hexagon while the red zone represents MoS₂.

Figure 4c shows the Raman mapping at A_{1g} mode of MoS_2 . Raman signal of MoS_2 can be obtained from the entire area of the sample. However, the Raman signal of the central area where CdS is grown is much weaker. This Raman mapping further demonstrates the epitaxial nature of the structure. The Raman spectra of the heterostructures are shown in Figure 4d. The peaks of E_{2g} mode at 383 cm^{-1} and A_{1g} mode at 402 cm^{-1} are the characteristic peaks of MoS_2 . On the other hand, the peaks at 212 cm^{-1} , 254 cm^{-1} , 300 cm^{-1} and 601 cm^{-1} are the characteristic peaks of CdS^[19]. The PL spectra of the heterostructures are shown in Figure 4e. We identified PL peak of MoS_2 at 1.81 eV. However, this peak disappeared after the formation of CdS/ MoS_2 heterostructure, accompanied by the appearance of a new peak at ~ 1.70 eV (Details on PL measurements using a 532 nm laser is presented in Figure S8, Supporting Information). The peak at 1.70 eV can be attributed to the interlayer excitonic transition of MoS_2 conduction band maxima to the CdS valence band minima.^[17] The three peaks in red line at 2.477 eV, 2.491 eV and 2.493 eV indicate the Raman peaks of Si, A_{1g} mode and E_{2g} mode of MoS_2 , respectively. The peak at 2.45 eV indicates the existence of CdS. Because CdS has a strong visible optical absorption, it is an attractive material for enhancement of light absorption and photoresponse of the heterostructure. UV-Vis-NIR absorption spectra of MoS_2 and CdS/ MoS_2 heterostructures are measured by transferring $0.5\text{ cm} \times 0.5\text{ cm}$ MoS_2 and CdS/ MoS_2 films on to glass substrates; Figure 4f. The coverage of CdS on MoS_2 is $\sim 20\%$, estimated from a series of SEM images. The plots indicate that the single layer MoS_2 has a weak light absorption and a small response scope (wavelength < 680 nm). Compared to MoS_2 , the CdS/ MoS_2 heterostructures have a much higher absorption and wider light response (wavelength < 1000 nm). The higher absorption and stronger response

can be explained by the band structure of the heterostructure; Figure 4g.^[27] Due to lower conduction band edge of MoS₂, electrons located in the conduction band of CdS tend to transfer to the conduction band of MoS₂, which leads to effective separation of electron-hole pairs and prevents the electron-hole recombination. Therefore, the number of carriers increases in the circuit, leading to the enhancement of photocurrent. We note that the broadening of response wavelength of the heterostructure is expected to reach to up to 730 nm after the formation of the vertical heterostructure. However, the UV-Vis-NIR spectra of the CdS/MoS₂ heterostructures indicates absorbance above 730 nm. This is likely due to the variation in shape, size and thickness of the CdS nanocrystals.

The single-layer MoS₂ and CdS/MoS₂ heterostructure-based photodetectors are fabricated using Ti/Au contacts on silicon substrates covered with 300 nm silicon oxide (SiO₂/Si). Figure 5a presents a schematic diagram of a single-layer MoS₂ photodetector with epitaxially grown CdS. The inset shows an optical microscope image of the actual device. The photoelectrical characterizations are measured at room temperature in ambient condition. As shown in Figure 5b, the photocurrent as a function of time is measured under alternative dark and illumination condition at 0.266 mW/cm², with a bias voltage $V_{ds} = 1V$ and a gate voltage $V_g = 0V$. At 610 nm (other wavelengths are shown in supporting information) ON and OFF illumination, both the single-layer MoS₂ and CdS/MoS₂ heterostructure-based photodetectors exhibit repeatable and stable response to the light. The response (light ON) and recovery (light OFF) time is calculated by averaging the device response and considering the time it takes to reach 80% of the final values. The measured rise time is 100 ms, much faster than that of the devices based on CVD grown single-layer MoS₂ (rise time >10 s). Compared to the

MoS₂ photodetector, the CdS/MoS₂ devices exhibit strong photocurrent enhancement under this illumination. Here, photocurrent (ΔI) is defined as the difference between I_{ON} and I_{OFF} with a voltage bias of 1V. Figure 5c shows the photocurrents of the MoS₂ and CdS/MoS₂ photodetectors under light with a series of wavelengths (365 nm, 490 nm, 550 nm, 610 nm and 700 nm). The photocurrent from MoS₂-based device gradually drops with the increase in wavelength, while that of the CdS/MoS₂-based device rises fast and reaches the maximum at 700 nm. Note that there is no significant response to light when the illumination wavelength is longer than the optical band gap of the single layer MoS₂ (1.82 eV, $\lambda = 681$ nm). This is because only the incident photons with energies exceeding 1.82 eV excite electrons from the valence band into the conduction band of MoS₂. CdS has a band gap of 2.45 eV. Thus the CdS photodetector is not expected to respond to >506 nm. However, we observe photoresponse of the CdS/MoS₂ detector at >680 nm. We propose that the photoresponse in this forbidden optical absorption region for pristine MoS₂ arises from the photoinduced electron transfer from the valence band of CdS to the bottom of conduction band of MoS₂.

Responsivity (R_λ) is another critical parameter to evaluate the performance of a photodetector. R_λ is defined as the photocurrent generated per unit power of the incident light on the effective device area. The value of R_λ can be calculated using the relation: $R_\lambda = \Delta I / P_\lambda S$. Here, ΔI is the generated photocurrent, P_λ is the incident light intensity, S is the effective illuminated area (In the present study $S \sim 1\text{mm} \times 20 \mu\text{m}$). The photo-responsivity under different wavelengths of MoS₂ and CdS/MoS₂ photodetectors is measured and the results is shown in Figure 5d. The results demonstrate that the epitaxial CdS plays an important role to enhance the photoresponsivity, with over 50 times increase in responsivity (70.8 mA/W Vs

3.91 A/W) under 610 nm illumination. Such a strong enhancement in photoresponsivity and simple device configuration underscores the potential application of this CdS/MoS₂ heterostructure.

3. Conclusions

In summary, we have demonstrated successful epitaxial growth of non-layered CdS on to MoS₂ to fabricate their vertical heterostructures using a one-step CVD method. We propose that the substrate surface energy plays an important role in the growth of CdS. We further demonstrate CdS/MoS₂ heterostructure-based photodetectors. The photocurrent and photo-responsivity of CdS/MoS₂ heterostructure-based photodetectors are greatly enhanced, compared to their MoS₂ counterparts, making our strategy very attractive for high-performance optoelectronic devices.

4. Experimental Section

Characterizations: The as-grown CdS/MoS₂ heterostructures are characterized by scanning electron microscopy (SEM, Hitachi S-4200), AFM (Nanoscope IIIa Veeco), UV-Vis-NIR absorption (Hitachi U-4100), transmission electron microscopy (TEM, Tacnai-G2 F30, accelerating voltage of 300 kV) and Raman spectroscopy (LabRAM XploRA, power 0.15 mW, excitation wavelength 488 nm and 532 nm). The detectors are annealed at 200 °C for 30 min with 100 sccm Ar : H₂ (V/V=9/1) to reduce the resistance and improve the contact for the devices.

Electrical measurements: These devices are characterised using a semiconductor analyzer (Keithley 4200 SCS) combined with a Lakeshore probe station. Photoelectric data are obtained by using a 500 W xenon lamp as the light source. Mono-chromatic lights of 254-850 nm are obtained using optical filters. The intensities of the incident light source are measured by a power and energy meter (Model 372, Scientek). The photocurrent measurements are performed using the Lakeshore probe station and an HP 4140B Semiconductor Parameter Analyzer.

Supporting Information Supporting Information is available from the Wiley Online Library or from the author.

Acknowledgements

This work is supported by the National Natural Science Foundation of China (NSFC, No.61390502, 21373068), the National key Basic Research Program of China (973 Program) under Grant No. 2013CB632900. TH acknowledges support from a Royal Academy of Engineering Research Fellowship (Graphlex).

Received: ((will be filled in by the editorial staff))

Revised: ((will be filled in by the editorial staff))

Published online: ((will be filled in by the editorial staff))

References

- [1] Y. Ohno, D. K. Young, B. Beschoten, F. Matsukura, H. Ohno, D. D. Awschalom, *Nature* **1999**, 402, 790.
- [2] R. Gaska, J. W. Yang, A. Osinsky, Q. Chen, M. A. Khan, A. O. Orlov, G. L. Snider, M. S. Shur, *Appl. Phys. Lett.* **1998**, 72, 707.
- [3] K. S. Novoselov, A. K. Geim, S. V. Morozov, D. Jiang, Y. Zhang, S. V. Dubonos, I. V. Grigorieva, A. A. Firsov, *Science* **2004**, 306, 666.
- [4] S. Z. Butler, S. M. Hollen, L. Cao, Y. Cui, J. A. Gupta, H. R. Gutiérrez, T. F. Heinz, S. S. Hong, J. Huang, A. F. Ismach, E. Johnston-Halperin, M. Kuno, V. V. Plashnitsa, R. D. Robinson, R. S. Ruoff, S. Salahuddin, J. Shan, L. Shi, M. G. Spencer, M. Terrones, W. Windl, J. E. Goldberger, *ACS Nano* **2013**, 7, 2898; Q. H. Wang, K. Kalantar-Zadeh, A. Kis, J. N.

- Coleman, M. S. Strano, *Nat. Nanotechnol.* **2012**, 7, 699; M. Chhowalla, H. S. Shin, G. Eda, L. J. Li, K. P. Loh, H. Zhang, *Nat. Chem.* **2013**, 5, 263.
- [5] K. K. Kim, A. Hsu, X. Jia, S. M. Kim, Y. Shi, M. Dresselhaus, T. Palacios, J. Kong, *ACS Nano* **2012**, 6, 8583.
- [6] H. Liu, A. T. Neal, Z. Zhu, Z. Luo, X. Xu, D. Tománek, P. D. Ye, *ACS Nano* **2014**, 8, 4033.
- [7] A. K. Geim, I. V. Grigorieva, *Nature* **2013**, 499, 419.
- [8] L. Britnell, R. V. Gorbachev, R. Jalil, B. D. Belle, F. Schedin, A. Mishchenko, T. Georgiou, M. I. Katsnelson, L. Eaves, S. V. Morozov, N. M. R. Peres, J. Leist, A. K. Geim, K. S. Novoselov, L. A. Ponomarenko, *Science* **2012**, 335, 947.
- [9] T. Georgiou, R. Jalil, B. D. Belle, L. Britnell, R. V. Gorbachev, S. V. Morozov, Y.-J. Kim, A. Gholinia, S. J. Haigh, O. Makarovskiy, L. Eaves, L. A. Ponomarenko, A. K. Geim, K. S. Novoselov, A. Mishchenko, *Nat. Nanotechnol.* **2013**, 8, 100.
- [10] W. J. Yu, Y. Liu, H. Zhou, A. Yin, Z. Li, Y. Huang, X. Duan, *Nat. Nanotechnol.* **2013**, 8, 952.
- [11] R. Cheng, D. Li, H. Zhou, C. Wang, A. Yin, S. Jiang, Y. Liu, Y. Chen, Y. Huang, X. Duan, *Nano Lett.* **2014**, 14, 5590.
- [12] W. Gannett, W. Regan, K. Watanabe, T. Taniguchi, M. F. Crommie, A. Zettl, *Appl. Phys. Lett.* **2011**, 98, 242105.
- [13] Z. Liu, L. Song, S. Zhao, J. Huang, L. Ma, J. Zhang, J. Lou, P. M. Ajayan, *Nano Lett.* **2011**, 11, 2032.
- [14] X. Ling, Y.-H. Lee, Y. Lin, W. Fang, L. Yu, M. S. Dresselhaus, J. Kong, *Nano Lett.* **2014**, 14, 464.
- [15] G. W. Shim, K. Yoo, S.-B. Seo, J. Shin, D. Y. Jung, I.-S. Kang, C. W. Ahn, B. J. Cho, S.-Y. Choi, *ACS Nano* **2014**, 8, 6655.
- [16] Y. M. Shi, W. Zhou, A. Y. Lu, W. J. Fang, Y. H. Lee, A. L. Hsu, S. M. Kim, K. K. Kim, H. Y. Yang, L. J. Li, J. C. Idrobo, J. Kong, *Nano Lett.* **2012**, 12, 2784.
- [17] Y. Gong, J. Lin, X. Wang, G. Shi, S. Lei, Z. Lin, X. Zou, G. Ye, R. Vajtai, B. I. Yakobson, H. Terrones, M. Terrones, Beng K. Tay, J. Lou, S. T. Pantelides, Z. Liu, W. Zhou, P. M. Ajayan, *Nat. Mater.* **2014**, 13, 1135.
- [18] X. Zhang, F. Meng, J. R. Christianson, C. Arroyo-Torres, M. A. Lukowski, D. Liang, J. R. Schmidt, S. Jin, *Nano Lett.* **2014**, 14, 3047.
- [19] Q. H. Li, T. Gao, T. H. Wang, *Appl. Phys. Lett.* **2005**, 86, 193109; Y.-F. Lin, J. Song, Y. Ding, S.-Y. Lu, Z. L. Wang, *Adv. Mater.* **2008**, 20, 3127.
- [20] C. Tan, H. Zhang, *J. Am. Chem. Soc.* **2015**, 137, 12162; C. Tan, H. Zhang, *Chem. Soc. Rev.* **2015**, 44, 2713.
- [21] S. H. Shah, A. Azam, M. A. Rafiq, *Cryst. Growth. Des.* **2015**, 15, 1792.
- [22] H. Zhou, F. Yu, C. F. Guo, Z. Wang, Y. Lan, G. Wang, Z. Fang, Y. Liu, S. Chen, L. Sun, Z. Ren, *Nanoscale* **2015**, 7, 9153.
- [23] J. Zhang, M. Brehm, M. Grydlik, O. G. Schmidt, *Chem. Soc. Rev.* **2015**, 44, 26; G. Chuan Fei, W. Yongsheng, J. Peng, C. Sihai, M. Junjie, Z. Zhuwei, L. Qian, *Nanotechnology* **2008**, 19, 445710; J. Liao, B. Sa, J. Zhou, R. Ahuja, Z. Sun, *J. Phys. Chem. C* **2014**, 118, 17594.
- [24] H. Heo, J. H. Sung, G. Jin, J.-H. Ahn, K. Kim, M.-J. Lee, S. Cha, H. Choi, M.-H. Jo, *Adv. Mater.* **2015**, 27, 3803.

- [25] J. N. Coleman, M. Lotya, A. O'Neill, S. D. Bergin, P. J. King, U. Khan, K. Young, A. Gaucher, S. De, R. J. Smith, I. V. Shvets, S. K. Arora, G. Stanton, H.-Y. Kim, K. Lee, G. T. Kim, G. S. Duesberg, T. Hallam, J. J. Boland, J. J. Wang, J. F. Donegan, J. C. Grunlan, G. Moriarty, A. Shmeliov, R. J. Nicholls, J. M. Perkins, E. M. Grieveson, K. Theuwissen, D. W. McComb, P. D. Nellist, V. Nicolosi, *Science* **2011**, 331, 568.
- [26] J. Mizele, J. L. Dandurand, J. Schott, *Surf. Sci.* **1985**, 162, 830; R. Cabriolu, P. Ballone, *Phys. Rev. B* **2010**, 81, 155432.
- [27] S. H. Yu, Y. Lee, S. K. Jang, J. Kang, J. Jeon, C. Lee, J. Y. Lee, H. Kim, E. Hwang, S. Lee, J. H. Cho, *ACS Nano* **2014**, 8, 8285; J. A. Herron, J. Kim, A. A. Upadhye, G. W. Huber, C. T. Maravelias, *Energ. Environ. Sci.* **2015**, 8, 126.

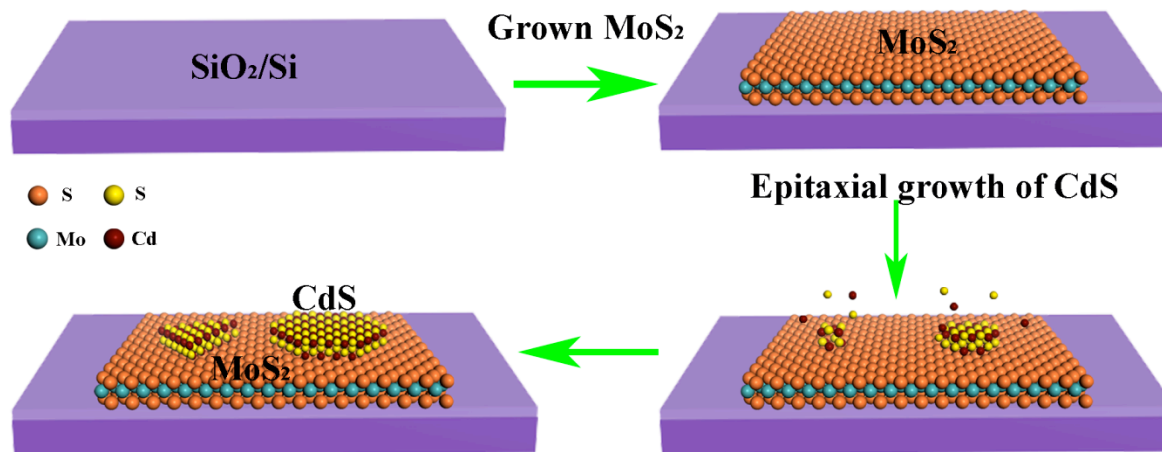


Figure 1. Schematic illustration of one-step epitaxial growth of CdS/MoS₂ heterostructures.

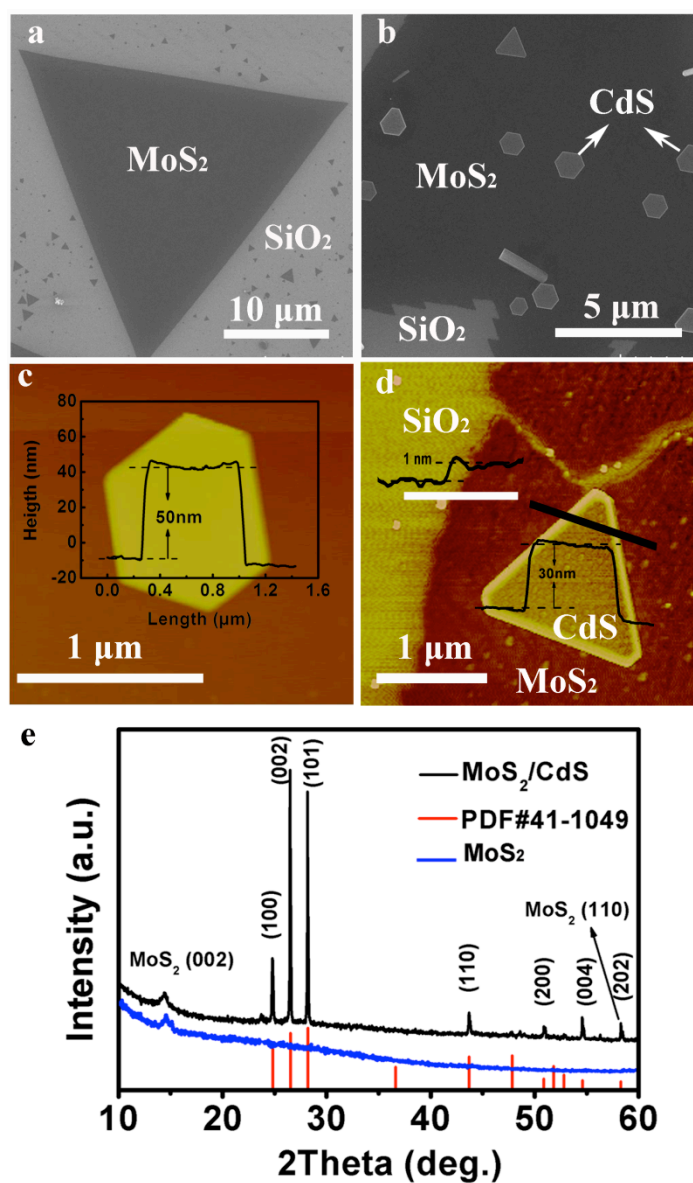


Figure 2. Characterization of vdW epitaxial CdS/MoS₂. (a, b) SEM images of CVD grown triangle MoS₂ and CdS/MoS₂ heterostructures, respectively. (c) AFM image and associated height profile of a hexagonal CdS. (d) AFM phase image of the heterostructure with associated height profiles. (e) XRD characterization of MoS₂ and CdS/MoS₂.

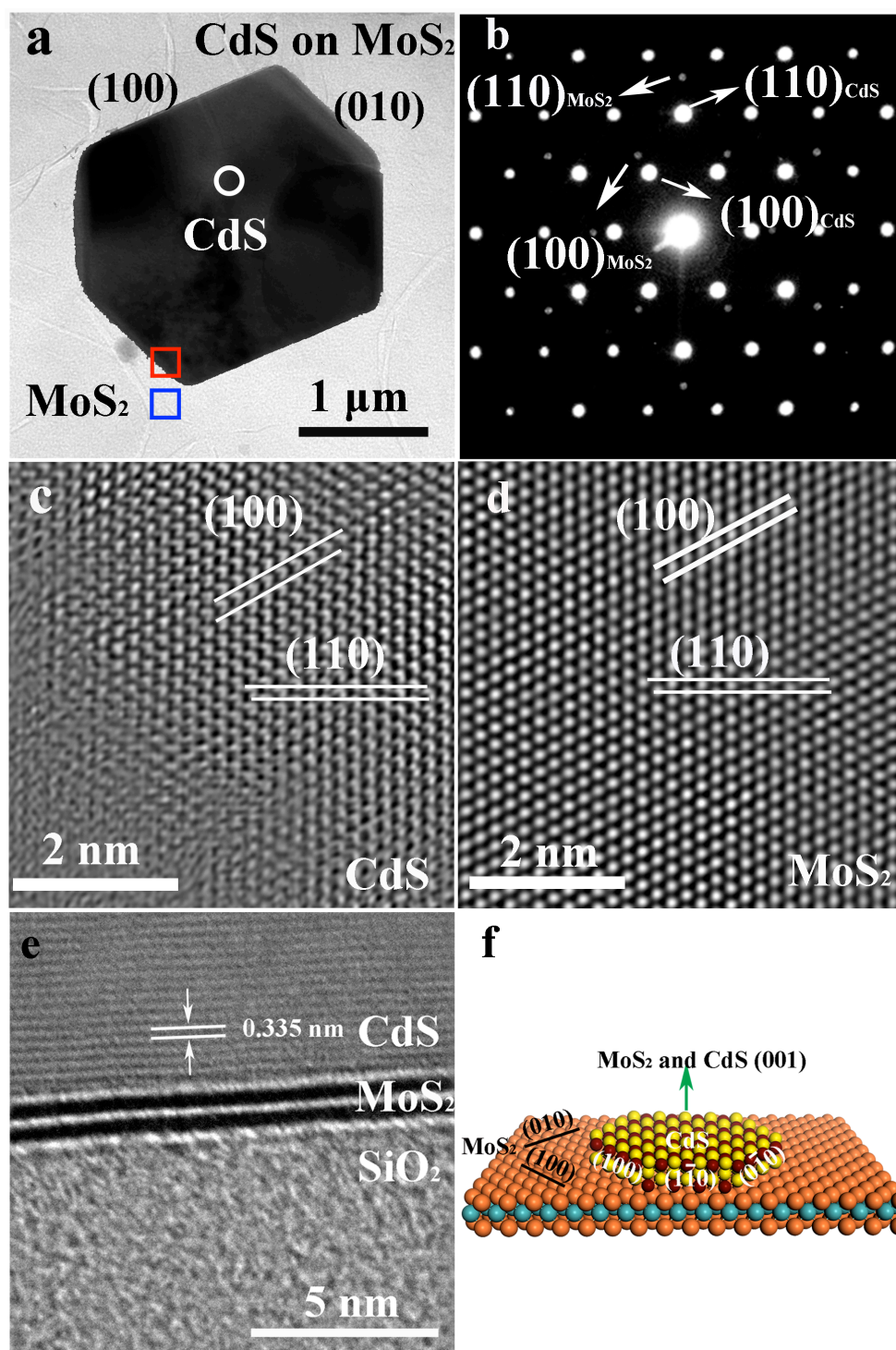


Figure 3. TEM characterization of the heterostructures. (a) Low-magnification TEM images of CdS/MoS₂ heterostructures. (b) Selected area electron diffraction (SEAD) of heterostructures. (c, d) Fast Fourier transform images of CdS and MoS₂, respectively. (e) Cross-sectional TEM images of the CdS/MoS₂ heterostructure. (f) Schematic model of the CdS/MoS₂ heterostructures.

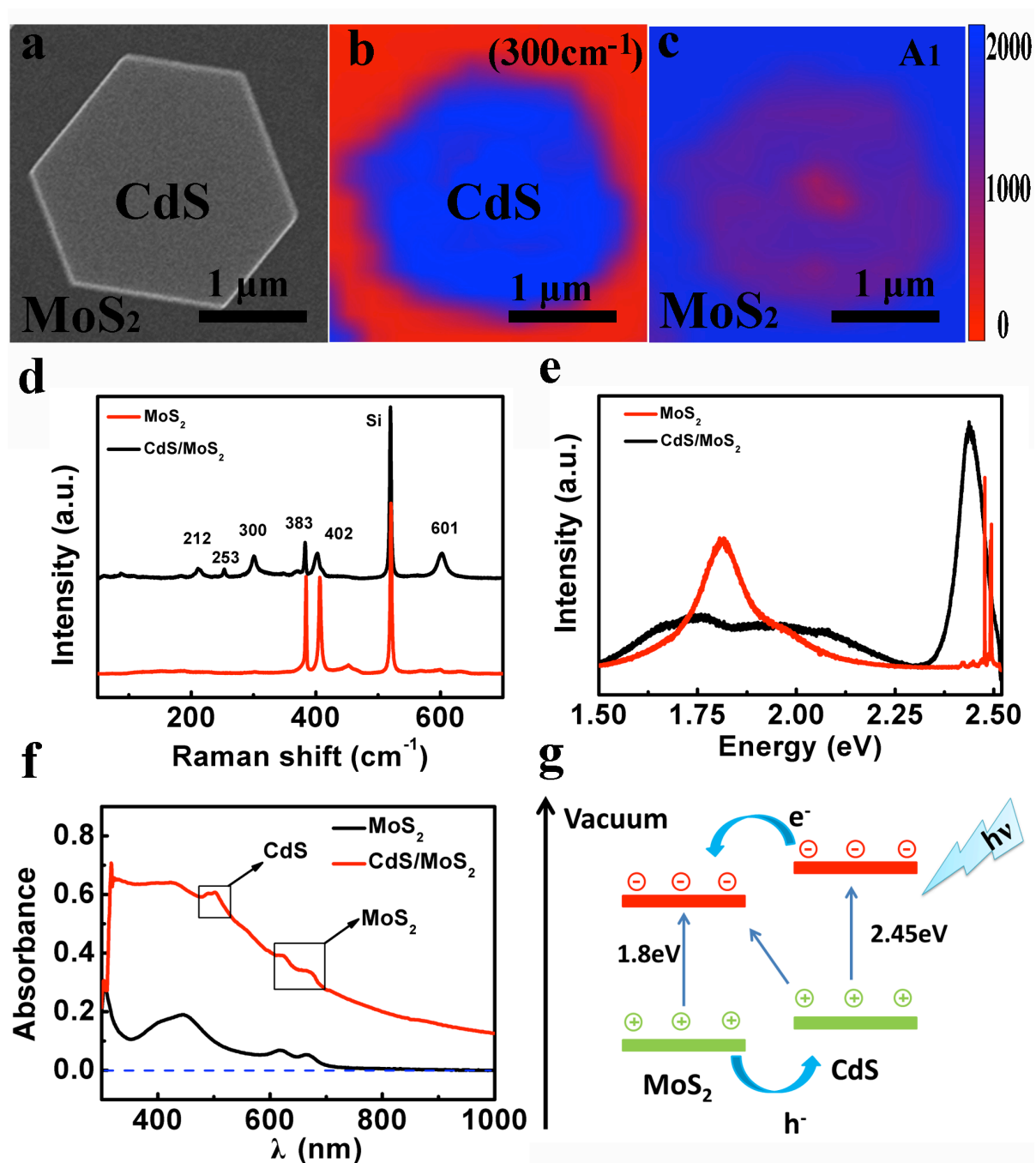


Figure 4. Spectroscopic characterizations of the as-grown CdS/MoS₂ heterostructures. (a) SEM image of hexagonal CdS on MoS₂. (b) Raman mapping of CdS at 300 cm⁻¹. (c) Raman mapping of MoS₂ at 402.1 cm⁻¹ (d, e) Raman and PL spectrum of the CdS/MoS₂ heterostructures. (f) UV-Vis-NIR spectrum of the CdS/MoS₂ heterostructures and single-layer MoS₂. (g) Band gap schematic of CdS/MoS₂ heterostructure photodetector under illumination.

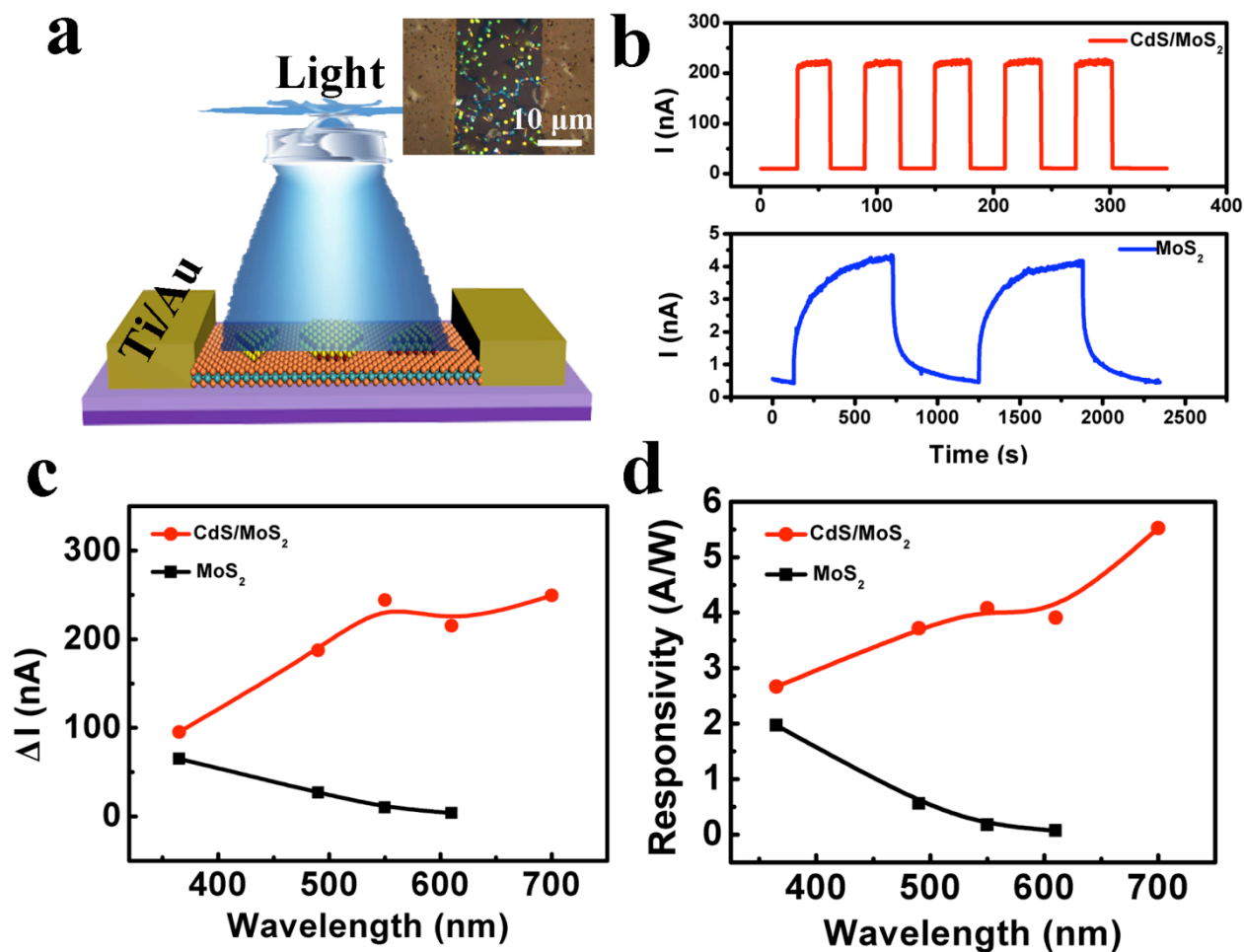


Figure 5. Characterizations of the photodetectors. (a) Schematic of CdS/MoS₂ heterostructure photodetector; inset shows an optical microscope image of the device. (b) Time-dependent photoresponse of CdS/MoS₂ heterostructure and single-layer MoS₂ photodetectors under 610 nm illumination, with a 1 V bias. (c, d) Photocurrent and photo-responsivity under 365, 490, 550, 610 and 700 nm wavelength of the same devices.

A new van der Waals heterostructure consisting of CdS nanosheet and MoS₂ via CVD process is presented. This is the first demonstration where a non-layered semiconductor has been epitaxially grown on to 2D layered crystal to fabricate a new type of van der Waals heterostructure. Compared to MoS₂ photodetectors, the photocurrent and photo-responsivity of CdS/MoS₂ heterostructure photodetector show significant enhancement.

Keywords: epitaxial growth, CdS/MoS₂ heterostructure, photodetector, responsivity

Wei Zheng, Wei Feng, Xin Zhang, XiaoShuang Chen, Guangbo Liu, Yunfeng Qiu, Tawfique Hasan, Pingheng Tan, PingAn Hu*

Anisotropic growth of non-layered CdS on MoS₂ monolayer for functional vertical heterostructures

ToC figure

